INSTITUTE OF PHYSICS PUBLISHING JOURNAL OF MICROMECHANICS AND MICROENGINEERING

J. Micromech. Microeng. **17** (2007) 350–357 doi:10.1088/0960-1317/17/2/022

Analysis and design of kinked (bent) beam sensors

Matthew R Begley[1] **and N Scott Barker**[2]

[1] Department of Mechanical and Aerospace Engineering, University of Virginia, Charlottesville, VA 22904, USA
[2] Department of Electrical and Computer Engineering, University of Virginia, Charlottesville, VA 22904, USA

Received 8 August 2006, in final form 12 October 2006
Published 19 January 2007
Online at stacks.iop.org/JMM/17/350

Abstract
This paper describes microfabricated freestanding 'v'-shaped beams, which may be used for a wide variety of sensing applications, e.g., temperature, residual stress arising from microfabrication and surface stresses generated by molecular adsorption. Analytical solutions are derived that connect structural deformation (i.e. output displacement) to physical driving forces and geometry. Various asymptotic limits are presented to illustrate the range of geometries for which bending and axial deformation can be neglected. An intriguing implication of the analysis is that the most sensitive device is only slightly kinked, with a kink angle close to the width-to-length ratio of the beams. For such structures, the displacements produced by buckling-type deformation can be much larger than those produced by purely axial elongation of structures with larger kink angles. The paper concludes with a discussion of the implications for designing highly sensitive devices, with an emphasis on the advantages of exploiting nonlinear behavior and constructing polymeric structures.

1. Introduction

An emerging strategy for microfabricated sensors is to construct slender 'v'-shaped beams, such as those shown in figure 1(*a*) (e.g. [1–4]). The central concept is to translate stresses generated along the axes of the freestanding beams into in-plane displacements along the symmetry plane, as shown schematically in figure 1(*b*). This geometry has two notable advantages. First, the in-plane asymmetry eliminates the need for additional layers to drive out-of-plane deformation (e.g. wafer curvature). This is a distinct advantage when quantifying mechanical properties (such as modulus, coefficient of thermal expansion (CTE) and residual stress) in microfabricated devices, as additional layers often introduce additional unknown parameters [5]. Moreover, additional layers can significantly decrease the performance of the device. For example, they can decrease the sensitivity to adsorption while increasing the sensitivity to temperature [6]. Related to this, the asymmetry of the structure implies that single-sided adsorption is not necessary: this not only facilitates surface functionalization but also increases sensitivity because the entire surface of the structure is utilized. Secondly, the structural asymmetry increases sensitivity over straight devices that exploit buckling (e.g. [7, 8]), and induces a directional bias that facilitates transduction. The in-plane deformation can be easily monitored using vernier scales (as shown in figure 1(*a*)) or capacitance gauges that are tuned to the displacement range of interest.

Perhaps the central challenge faced in the design of high performance sensors is quantifying the connection between structural deformation and physical inputs, such as residual stress, temperature changes and surface stresses generated by molecular adsorption. Previous efforts have outlined the essential elements of the analysis, design and fabrication kinked beam sensors to measure residual stress [1, 2] and thermal expansion coefficient [3]. However, they do not clearly identify key relationships between sensitivity, geometry (including kink angle) and material choice. This is especially true for nonlinear regimes where buckling-type behavior plays an important role. Here, we present comprehensive analytical solutions describing deformation for a variety of physical inputs that span both linear and nonlinear behaviors. The new closed-form solutions presented here enable one to identify optimal kink angles and aspect ratios that maximize sensitivity. This comprehensive framework is then used to discuss the choices of geometry and materials that

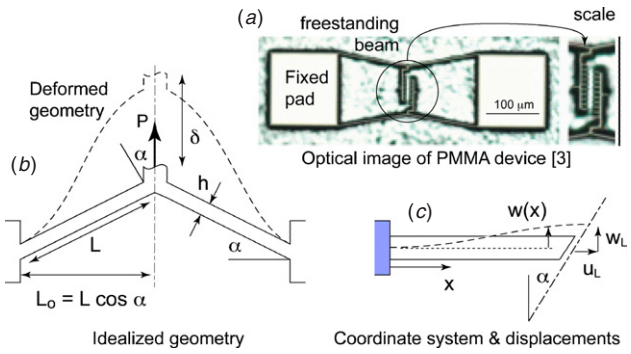

Figure 1. (*a*) Optical micrograph of a microfabricated kinked beam sensor, (*b*) idealization of the bottom half of the sensor and (*c*) coordinates and deformation variables used in the analysis. The coordinate system in (*c*) is aligned with the kinked beam, i.e. rotated from the global coordinate system in (*b*).

(This figure is in colour only in the electronic version)

lead to highly sensitive devices, in the context of molecular adsorption and temperature.

2. Mechanics

The idealized model for the kinked (bent) beam sensor shown in figure 1(*a*) is shown schematically in figures 1(*b*) and (*c*). Figure 1(*b*) illustrates the idealized geometry for the bottom half of the structure shown in figure 1(*a*); the load aligned with the symmetry axis, P, represents an external point force acting on the tip of the v-shaped structure. (For example, this load may arise from electrostatic actuation of a comb drive, or if the sensor is used as a mechanical probe.) Figure 1(*c*) shows the one-half of each v-shaped beam, with the centerline of the beam (i.e. the x-axis) rotated to be strictly horizontal. As such, the vertical symmetry condition in figure 1(*b*) corresponds to an inclined roller condition at the end of the beam shown in figure 1(*c*). Figures 1(*b*) and (*c*) illustrate a 'clamped' condition, for which the tangent of the deformed beam at the symmetry axis is parallel to the original centerline of the beam.

It is assumed that the arms of the sensor behave as beams, in that the direct stresses in both the y- and z-directions are negligible compared to the direct stresses in the x-direction. The degree of rotational constraint at the ends—i.e. along the symmetry line and at the pad connection—obviously depends on the details of the geometry at these 'joints'. This is accounted for by adjusting the boundary conditions applied at the ends, as detailed below. In the limit of a zero kink angle, the response reduces to that of the straight beam, discussed in detail in [7, 9].

In section 2.1, the general governing equations are defined. Scenarios with tensile and compressive axial resultants must be considered independently, because the nature of the solution to (3) changes with the sign of N. Section 2.2 presents suitable normalizations and solutions, while important asymptotic limits are outlined in section 2.3.

2.1. General framework

The beams are described using the one-dimensional version of nonlinear von Karman plate theory; in this approach, the deformation of the beam is described by

$$\varepsilon_{xx}(x) = u'(x) + \tfrac{1}{2}(w'(x))^2 - yw''(x), \tag{1}$$

where $u(x)$ is the axial displacement of the centerline, $w(x)$ is the transverse displacement of the centerline (in the y-direction), y is the distance from the centerline and the primes denote differentiation with respect to the x-direction. The second (nonlinear) term accounts for moderate rotations, which can generate significant stretching of the centerline (when displacements are comparable to the beam thickness).

The strain term ε_o describes the role of any physical mechanism that generates axial strain when the beam is not constrained (or otherwise loaded), such as intrinsic stress, thermal expansion, surface stresses, fluid-induced swelling, etc. Thus,

$$\varepsilon_o \equiv \Delta\alpha\Delta T - \frac{\sigma_o}{E} - \frac{2\gamma(b+h)}{Ebh}, \tag{2}$$

where E is the elastic modulus, $\Delta\alpha \equiv \alpha - \alpha_s$ is the differential coefficient of thermal expansion relative to the substrate, $\Delta T = T - T_o$ is the temperature change from the reference temperature (at which thermal strains are zero), σ_o is the intrinsic stress arising from fabrication, γ is a surface stress (as might be generated by molecular adsorption), h is the beam width (or height in the bending direction) and b is the thickness of the beam in the z-direction.

A potential source of confusion in the subsequent analysis is the sign convention adopted for intrinsic and/or thermal stresses, since the nature of the solution changes with the sign of the axial force in the beam. According to the above definitions, the average axial stress in the beam is given by

$$\sigma(x) = E\big(u'(x) + \tfrac{1}{2}(w'(x))^2 - \varepsilon_o\big). \tag{3}$$

This can be used to clearly explain the sign conventions. Consider the case of a perfectly flat beam, such that $w'(x)$ is identically zero. For a cantilever, $\sigma(x) = 0$, such that the axial displacement gradient is $u'(x) = \varepsilon_o$. Clearly, $\Delta\alpha\Delta T > 0$ leads to elongation, while $\sigma_o < 0$ and $\gamma < 0$ each correspond to compressive stresses that are balanced by stretching of the beam. Conversely, if a beam is clamped between rigid walls, $u'(x) = 0$, such that the stress in the beam is given by $\sigma(x) = -E\varepsilon_o$. Thus, increases in temperature lead to compressive stresses, as do $\sigma_o < 0$ and $\gamma < 0$.

The fabrication stress σ_o represents intrinsic stress that may arise during deposition or curing, but may be defined to include any thermal stress contribution arising from deposition at an elevated temperature. In the latter approach, the temperature change should be defined relative to the ambient temperature of device operation.

The governing equations for deformation can be obtained by utilizing equation (1) in a variational approach that renders the potential energy stationary [9]. This yields

$$\frac{Ebh^3}{12}w^{IV} - bh\sigma(x)w'' = 0. \tag{4}$$

The second governing equation obtained via the variational approach is

$$\big(u'(x) + \tfrac{1}{2}(w'(x))^2\big)' = 0. \tag{5}$$

For spatially uniform input strains ε_o, equations (3) and (5)

imply $\sigma'(x) = 0$. Thus, the average axial stress is constant along the length of the beam. This has the fortuitous effect of reducing equation (4) to a linear ordinary differential equation. To simplify the notation, $\sigma(x)$ is replaced with σ, a constant to be determined.

The solution involves five constants: four arising from the solution to equation (4) and the unknown average axial stress, σ. The boundary conditions at either end of the beam relating to transverse displacement and its derivatives provide four additional equations; the fifth and final boundary condition is dictated by the displacement constraint along the axis of symmetry. Along the centerline,

$$u_L = w_L \tan\alpha, \tag{6}$$

where u_L and w_L are the axial and transverse displacements at the end of the beam, respectively. The axial displacements along the centerline are obtained by integration of equation (3) with $y = 0$. Along the symmetry line of the device (at $x = L$), the coupling between axial and transverse displacements is described by

$$L\left(\frac{\sigma}{E} + \varepsilon_o\right) - \frac{1}{2}\int_0^L (w')^2\,\mathrm{d}x = w(L)\tan\alpha. \tag{7}$$

The second term in equation (7) represents the axial displacements that arise from transverse deflections.

Regardless of the constraint against rotation provided by the center block, the shear force aligned along the axis of symmetry must be equal to any applied load at the tip of 'v'. Elementary force equilibrium along the symmetry line at the right end ($x = L$) implies the following condition:

$$N(\tan\alpha + w') + V(1 - w'\tan\alpha) = P/2, \tag{8}$$

where $V = -Ebh^3 w'''/12$ is the shear force resultant, $N = bh\sigma$ is the axial force resultant and P is an external point load applied to the tip of 'v'. The boundary conditions at either end relating to rotation of the beam at the joint can be accounted for in a general way with the relation

$$M = \frac{Ebh^3}{12} w'' = k_t w', \tag{9}$$

where M is the resultant moment acting at the symmetry plane and k_t is the torsional spring constant which represents the joint's resistance to rotation. There are two obvious limiting cases: when $k_t \ll Ebh^3$, the joint provides no resistance to bending and the boundary condition is $w'' = 0$. At the other extreme, the end is effectively clamped because $k_t \gg Ebh^3$, such that the boundary condition is $w' = 0$.

These two cases bracket all possible behaviors, and as such dictate minimum and maximum possible deflections. In the rest of the paper, the focus is placed on clamped conditions, since these yield lower bound estimates for displacement. An exception is made for small deflection scenarios, for which a closed-form solution that incorporates equation (9) can be easily derived.

Finally, it should be noted that the displacement of the block *in the direction of the symmetry line* at $x = L$ is given by

$$\delta = \frac{w(L)}{\cos\alpha}. \tag{10}$$

2.2. Normalized governing equations and solutions

With suitable normalization, the governing equations become

$$\hat{w}^{IV} \mp \lambda^2 \hat{w}'' = 0, \tag{11a}$$

$$\varepsilon_0 - \frac{1}{2}\int_0^1 (\hat{w}')^2\,\mathrm{d}\bar{x} \pm \frac{\bar{h}^2}{12}\lambda^2 = \hat{w}(1)\tan\alpha, \tag{11b}$$

$$(1 - w'\tan\alpha)\hat{w}''' \pm \lambda^2(w' + \tan\alpha) = \hat{P}, \tag{11c}$$

where the top sign is used if $\sigma > 0$ (tensile stress in the beam, $\lambda^2 > 0$), and the bottom sign is used if $\sigma < 0$ (compressive stress in the beam, $\lambda^2 < 0$). The normalizations are

$$\lambda = \sqrt{\frac{12|\sigma|L^2}{Eh^2}}, \qquad \hat{P} = \frac{6PL^2}{Ebh^3}, \qquad \hat{w} = w/L,$$
$$\bar{x} = x/L, \qquad \bar{h} = h/L. \tag{12}$$

Of the two possible limits for constraint along the line of symmetry (i.e. clamped, or $w'(1) = 0$, or pinned, $w''(1) = 0$), the clamped condition represents the minimum deflection. Fortuitously, it also leads to far simpler algebra. Hence, solutions are presented for $w'(0) = w'(1) = 0$, which assumes that the ends of the beam are constrained against rotation from their initial orientation.

For the tensile regime ($\lambda^2 > 0$) one obtains the following result for the displacement along the symmetry axis, after some algebraic gymnastics:

$$\hat{\delta} = \frac{1}{\lambda^3}\left(\frac{\sec h\left(\frac{\lambda}{2}\right)}{\cos^2\alpha}\right)(\hat{P} - \lambda^2\sin\alpha) \times \left(\lambda\cosh\left(\frac{\lambda}{2}\right) - 2\sinh\left(\frac{\lambda}{2}\right)\right), \tag{13a}$$

where the value of λ (corresponding the axial resultant in the deformed state) is dictated by

$$\varepsilon_o + \frac{\bar{h}^2\lambda^2}{12} + \frac{\sec^2\alpha}{2\lambda^4\cosh^2\left(\frac{\lambda}{2}\right)}(\hat{P}^2 - \lambda^2\sin\alpha)^2 \times \left(2 + \cosh\lambda - \frac{3\sinh\lambda}{\lambda}\right) - \frac{\tan\alpha\sec\alpha}{\lambda^3\cosh\left(\frac{\lambda}{2}\right)} \times (\hat{P}^2 - \lambda^2\sin\alpha)\left(\lambda\cosh\left(\frac{\lambda}{2}\right) - 2\sinh\left(\frac{\lambda}{2}\right)\right) = 0. \tag{13b}$$

For the compressive regime ($\lambda^2 < 0$) one obtains different results, due to the changes of signs in equations (11*a*)–(11*c*). The sign of the axial stress is accounted for in equations (11*a*)–(11*c*); hence, in the following, σ represents the *magnitude* of the *compressive* stress in the beam, as is typical in buckling analyses. The displacement along the symmetry axis is given by

$$\hat{\delta} = -\frac{\sec^2\alpha\tan\alpha}{\lambda}\left(\lambda - 2\tan\left(\frac{\lambda}{2}\right)\right). \tag{14a}$$

The axial stress in the beam is determined by the solution to

$$\varepsilon_o - \frac{\bar{h}^2\lambda^2}{12} + \frac{\sec^2\alpha\cos^2\left(\frac{\lambda}{2}\right)}{2\lambda^5}(\hat{P}^2 + \lambda^2\sin\alpha)^2 \times (2\lambda + \lambda\cosh\lambda - 3\sinh\lambda) + \frac{\tan\alpha\sec\alpha}{\lambda^3} \times (\hat{P}^2 + \lambda^2\sin\alpha)\left(\lambda - 2\tan\left(\frac{\lambda}{2}\right)\right) = 0, \tag{14b}$$

where again, it should be noted that no adjustment to signs is necessary to account for $\sigma < 0$, since the sign is accounted

for in the governing equations and σ is reinterpreted as the magnitude of compressive stress.

The output displacement, $\hat{\delta}$, can be determined for given physical inputs (i.e. ε_o and $\hat{P}$) by a numerical solution of equation (13*b*) or (14*b*) and back substitution into equation (13*a*) or (14*a*). Alternatively, one can determine displacements parametrically, by specifying (λ, ε_o) and determining the corresponding $(\hat{\delta}, \hat{P})$ via direct evaluation of equations (13) and (14). Both of these approaches are facilitated by understanding the asymptotic behavior of these equations, which is described next.

2.3. Asymptotic results for small deflections and purely kinematic deformation

Elementary beam theory, which neglects axial/transverse coupling entirely, can be used to derive results for small deflections, i.e. linear solutions appropriate for small ε_o and $\hat{P}$. In this limit, it is trivial to include the possibility of beam rotation at the symmetry line (i.e. to impose equation (9) as a boundary condition). Thus, a broadly general result is

$$\frac{\sigma}{E} = \frac{\bar{h}^2}{12}\lambda^2 = \frac{\left(-\bar{h}^2\varepsilon_o + \frac{\hat{P}\bar{h}^2}{12}\sec\alpha\tan\alpha\right)}{\left\{\frac{1+\hat{k}}{4+\hat{k}}\right\}\bar{h}^2 + \tan^2\alpha} \tag{15}$$

and

$$\hat{\delta} = \frac{\left(\frac{\hat{P}\bar{h}^2}{12} + \varepsilon_o\sin\alpha\right)}{\left\{\frac{1+\hat{k}}{4+\hat{k}}\right\}\bar{h}^2\cos^2\alpha + \sin^2\alpha}, \tag{16}$$

where the normalized torsional spring constant reflecting the joint's resistance to rotation is given by

$$\hat{k} \equiv \frac{12k_tL}{Ebh^3}. \tag{17}$$

Clearly, the pre-factor of the $\bar{h}^2$ terms in the denominators of equations (15) and (16) reflects the importance of bending deformation, and varies between $\frac{1}{4}$ (i.e. a 'pinned' joint with $k_t = 0$) and unity (i.e. a 'clamped' joint with $k_t \to \infty$). It should be noted that equation (16) provides a closed-form expression to describe the *initial* 'incremental sensitivity' and 'incremental ratio of bending' illustrated graphically in [1].

Equations (15) and (16) are applicable for small displacements, regardless of the sign of external physical inputs. They also clearly produce the correct asymptotic limits. For example, for a straight beam ($\alpha = 0$), the axial stress is simply $\sigma = -E\varepsilon_o$, i.e. bending does not play a role; one recovers the elementary displacement result for a point-loaded beam of length $2L$, i.e. $\hat{\delta} = \hat{P}/12$. For a needle-like vertical structure ($\alpha = \pi/2$), $\sigma = P/2bh$ and $\hat{\delta} = P/(2Ebh) + \varepsilon_o$, which are the obvious limits for an axial bar (noting that the total load P acts on two cross-sections of dimension $b \times h$).

One can also obtain equations (15) and (16) for $k_t \to \infty$ by expanding equations (13*a*) and (13*b*) in a series about $\lambda = 0$. In order to obtain results identical to the elementary beam theory result—wherein the axial and horizontal equilibrium equations are decoupled—one must neglect terms of $O(\hat{P}^2, \hat{P}\lambda^2)$[3]. Identical results are obtained from equation (14), though one must note the difference in sign convention dictated by reinterpreting σ as the magnitude of compressive stress. The above asymptotic limits (for axial stress and displacement) represent the most generally applicable limit, in that they are valid for all values of α. However, they clearly do not capture any coupling between axial and transverse deflection. As a result, they are particularly prone to error in predicting the deflection of the structure in response to the external load P; this response is strongly influenced by the relative magnitudes of ε_o, $\bar{h}$ and $\hat{P}$, which all may be of the same order. This makes it difficult to compare the relative magnitudes of nonlinear terms in any series expansion.

A second limit of interest is a purely kinematic structure for which bending deformation and axial stress are negligible. Such a structure consists of two links pinned at the center and both ends; the axial strain in the links is simply ε_o. This solution is dictated purely by geometry and is given by

$$\hat{\delta} = \sqrt{\tfrac{1}{2} + \varepsilon_o(2+\varepsilon_o) - \tfrac{1}{2}\cos 2\alpha} - \sin\alpha. \tag{18}$$

This represents the maximum possible deflection because it ignores both neutral axis deformation and bending. Equation (18) illustrates that the behavior depends strongly on the relative size of the input strain ε_o and the kink angle α. When $\varepsilon_o \ll \alpha$, the response is linear with $\hat{\delta} \cong \varepsilon_o/\sin\alpha$; this is the same limit obtained from the full analysis (above) when $\bar{h} \to 0$ (i.e. bending is neglected). For very small kink angles, however, the response is inherently nonlinear; for example when $\alpha \ll \varepsilon_o$, then $\hat{\delta} \cong \sqrt{2\varepsilon_o}$. It must be emphasized that the accuracy of these limits are strongly dependent on the relative sizes of $\bar{h}$, ε_o and α.

3. Implications for device design and performance

The two fundamental design variables are the kink angle α and the aspect ratio of the beams, $\bar{h} = h/L$. The central challenge is to identify appropriate values to achieve the desired relationship between output displacement, $\hat{\delta} = \delta/L$, and the generalized input strain[4], ε_o. In many contexts, the ideal input/output relationship would be linear (i.e. $\hat{\delta} = m\varepsilon_o$), with a high sensitivity (i.e. large m). However, as will be demonstrated, these goals—linearity and sensitivity—are often in conflict with one another. The key to understanding this is to recognize that the input strain ε_o is quite small in most applications, i.e. ε_o typically ranges from 10^{-6} to 10^{-2}. As such, nonlinear regimes where $\hat{\delta} \propto \sqrt{\varepsilon_o}$ can lead to larger displacements than regimes where $\hat{\delta} \propto \varepsilon_o$. A fundamental characteristic of the kinked beam sensor is that the greatest sensitivity is achieved when α and $\bar{h}$ are both small and comparable.

Generally, the following discussion is limited to scenarios where the center joint is constrained against rotation (i.e. clamped), because this scenario produces the smallest sensitivity prediction. (That is, larger displacements are obtained for the same input when one assumes that the centerline acts as a pinned joint.) The exception is section 3.1, which provides a comparison of 'pinned' and clamped centerline boundary conditions in the limit of small deflections (i.e. linearized response). The nonlinear behavior of structures pinned at the centerline is qualitatively similar; quantitative differences are lower buckling thresholds and larger displacements.

[3] This necessity is easily recognized when one notes that $\hat{P}$ represents the load at which the deflection of a perfectly straight beam ($\alpha = 0$), is $\delta = L/12 \gg h$, a very large displacement that would lead to strong nonlinearity.

[4] To simplify the present discussion, the external load P is taken to be zero.

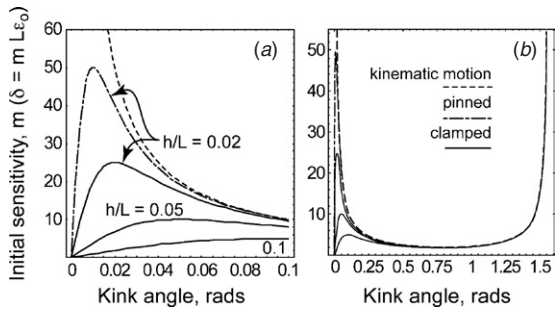

Figure 2. Initial sensitivity, m, of kinked beam sensors as the input strain approaches zero, i.e. $\varepsilon_o \to 0$; in this limit, the response is linear with $\hat{\delta} = m\varepsilon_o$: (*a*) results for small kink angles, (*b*) results for the entire range of kink angles.

3.1. Linear response: $\hat{\delta} = m\varepsilon_o$

For sufficiently small input strains and kink angles greater than h/L, the input/output behavior is linear, with the sensitivity m dictated by equation (16). Figures 2(*a*) and (*b*) illustrate the sensitivity as a function of kink angle for several aspect ratios. Because equation (16) includes the effects of rotational constraint at the symmetry line, results are shown for both clamped and pinned structures, which represent the extremes of response (i.e. maximum and minimum sensitivities). Unfortunately, 'sufficiently small' is difficult to define *a priori*, because the range of linear response is strongly dependent upon the kink angle. For very small kink angles (less than 5° or so), linear response is obtained for strain factors less than the buckling limit, which is defined in the following section. For larger kink angles, linear behavior can persist to input strains as large as 10^{-2}.

It is clear from both the figure and equation (16) that the optimum kink angle in this regime is given by $\alpha_o \cong \bar{h}, \pi/2 - 2\bar{h}$ for clamped structures, which for slender structures yields $m_o \cong L/2h$. The results in this figure correspond to the results for the initial sensitivity (i.e. at low stress) described in [1]; we note, however, that this previous work considers $\alpha \geqslant 0.05$ radians, and as such does not illustrate the decrease in sensitivity for sufficiently small kink angles as shown in figure 2. The larger angle with equal sensitivity, i.e. $\alpha_o = \pi/2 - 2\bar{h}$, corresponds to the angle at which the restoring moment (which is required to maintain the fixed slope at the kink and decreases output displacement) goes to zero. The upper envelope for the sensitivity is simply the small strain limit (i.e. $\varepsilon_o \ll \alpha$) of the purely kinematic result, i.e. equation (18): $m_k \cong 1/\sin\alpha$.

For sufficiently large kink angles, the response is independent of $\bar{h}$ and is characterized by purely kinematic rotation of the beams. It is interesting to note that the lower bound for kink angles that result in purely kinematic structures is relatively small, i.e. $\alpha_{k,\min} \approx 0.2$ rads $\approx 11°$, for values of $\bar{h}$ most relevant to microfabricated devices. However, it is important to note that the range of validity of the linear regime decreases with decreasing α, as implied by the competition between ε_o and α in equation (18). Physically, this simply means that for very small α, nonlinear deformation plays a significant role at decreasing values of ε_o.

For some (including the authors), the increase in sensitivity obtained for very small kink angles is counter-intuitive: one may initially suspect that larger kink angles provide less constraint and therefore enable larger displacements. This is certainly true for very large kink angles that correspond to 'needle'-like structures that are nearly vertical. However, the translation of axial input strain to transverse displacement for nearly straight beams is highly effective. This is easiest to understand by first considering the behavior of perfectly straight beams, i.e. buckling phenomena. Hence, this limit is discussed in section 3.2. However, in a nutshell, greater sensitivity is obtained for small kink angles—even in the linear regime—because the response is influenced by nonlinear strain–displacement relationships. The somewhat complicated transition from initially linear to nonlinear input/output relationships is discussed in section 3.3.

3.2. Purely nonlinear response obtained from $\alpha \equiv 0$

In the limit of perfectly straight beams, equations (13) and (14) yield classical buckling results. Attention is limited to cases where the center joint prevents rotations, i.e. a clamped boundary condition along the line of symmetry. A frequently overlooked fact is that the linear governing equation, equation (11*a*), when coupled with the nonlinear constraint relating to axial displacements, equation (11*b*), yields elegant closed-form solutions for post-buckling displacements[5]. The buckling displacement is given by

$$\hat{\delta} = \frac{4}{\pi}\sqrt{\varepsilon_o - \frac{\pi^2}{12}\left(\frac{h}{L}\right)^2}. \tag{19}$$

Clearly, the displacements should be taken as zero beneath the bifurcation limit, defined as $\varepsilon_{cr} = \frac{\pi^2}{12}\left(\frac{h}{L}\right)^2$.

The fact that the displacement is zero beneath the bifurcation limit leads to the presumption that buckling displacements are generally small. While they may indeed be small relative to the beam length, they are not generally *smaller* than displacements of moderately kinked beams (as is illustrated by results in the following section). The efficiency of buckling in generating transverse displacements is a consequence of the fact that the strain accommodated by transverse displacement scales as $\varepsilon \propto (\delta/L)^2$. (This can be inferred from the kinematic result equation (17), or alternatively, directly from equation (1) upon noting the deformed slope scales as $w' \propto \delta/L$.) Hence, the transverse displacement needed to accommodate the input strain scales as $\delta \propto \sqrt{\varepsilon_o}$. For small input strains, this implies that slender devices that exploit nonlinear buckling-type deformation can be quite effective in generating transverse displacements.

3.3. Transitions between linear and nonlinear responses

Figures 3 and 4 illustrate the output displacement as a function of input strain, for several values of kink angle and aspect ratio. Once again, attention is limited to cases where the center joint prevents rotations, i.e. a clamped boundary condition along the line of symmetry. Qualitatively similar results are obtained if

[5] Indeed, undergraduates are often instructed that solving for post-buckling displacements requires nonlinear analysis. Strictly speaking, this is true; however, the additional step of using the solution to the linear governing equation to evaluate equation (10*b*) seems well within their grasp.

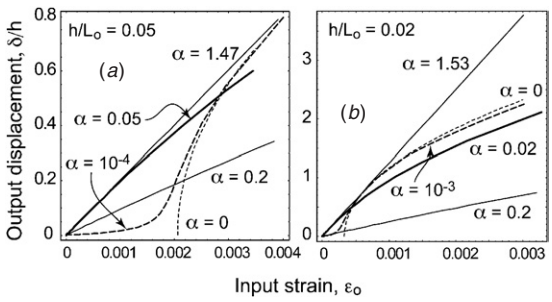

Figure 3. Input/output relationships for kinked beam sensors for two aspect ratios (with a constant pad-to-pad distance, $2L_o$) and several kink angles: (*a*) $h/L_o = 0.05$ and (*b*) $h/L_o = 0.02$; for fixed beam widths and pad distance, kink angles that equal the aspect ratio maximize initial sensitivity and provide large nonlinear displacements.

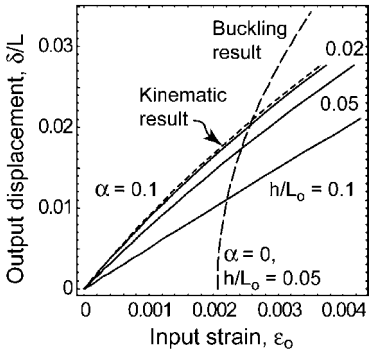

Figure 4. Input/output relationships for kinked beam sensors for several aspect ratios (with constant beam length, L, and constant kink angle, α); when the beam length and kink angle are fixed, the narrowest beam produces the largest displacement.

a pinned condition is imposed along the centerline, with lower buckling thresholds and generally larger displacements than the clamped case (as indicated by figure 2.)

The results compare devices with a fixed pad-to-pad distance, which equals $2L_o$ (see figure 1); for small angles, the distinction between L and L_o is negligible. Moreover, the output displacements are normalized by the beam width, h; as such, one must presume that the length is being varied in order to make meaningful comparisons regarding displacement magnitude. These figures are generated via a parametric plot of equations (14*a*) and (14*b*) (using *Mathematica*—*www.wolfram.com*). The striking feature of these results is that very small kink angles lead to larger displacements over physically reasonable ranges of input strain.

The initial slope of the curves (at zero input strain) is dictated by the linear response described in section 3.1. The slope of these curves at a specific strain level corresponds to the 'incremental sensitivity' of the device, as defined [1]. As previously illustrated for residual stress sensors, the incremental sensitivity can either increase or decrease with increasing input strains [1], as reflected by the changing slope in figures 3 and 4. Here, the curves demonstrate that this is true for compression in the beam. The results in [1] demonstrate this rise and fall in sensitivity for cases with tension in the beams, but do not consider sufficiently small kink angles to illustrate this effect for compression.

For shorter beams (i.e. larger h/L_o), the buckling threshold may be large compared to small input strains (see figure 3(*a*)), such that larger kink angles yield greater displacements. For more slender beams, the buckling threshold is much lower, such that small kink angles yield larger displacements for all physically realistic values of input strain (see figure 3(*b*)). Note that the results verify the completeness of the solution for all kink angles; one asymptotically obtains the classically buckling result for perfectly straight beams, and purely kinematic deformation for larger kink angles.

It is clear that the optimal kink angle for the linear regime (i.e. the kink angle that maximizes sensitivity as $\varepsilon_o \to 0$) produces an input/output relationship that is highly favorable. Not only is the initial sensitivity maximum, large displacements are generated for physically meaningful strains due to the inherent scaling relationships in the nonlinear regime. Put another way, the small kink angles dramatically improve the initial sensitivity of the device, while maintaining the large displacements generated by buckling-type behavior. Note again that these results are for fixed beam width, h, such that variation in parameters indicates changes in length of the beams.

Figure 4 illustrates the results for a single kink angle ($\sim 5^\circ$) and several values of beam width, h, and fixed beam length (since the kink angle is fixed). For the sake of comparison, the buckling result for a perfectly straight beam with $h/L_o \cong h/L = 0.05$ is also shown. In this figure, the displacement is normalized by the beam length to illustrate the effect of changing beam width. Clearly, one maximizes displacement by decreasing the beam width; ultimately, the purely kinematic result is obtained for very slender beams.

The choice of normalization in figure 4 demonstrates that the kink angle for maximum sensitivity depends on the choice of dimensions that are varied. When the beam length and angle are fixed (as in figure 4), the maximum sensitivity is always obtained for minimum beam width. In contrast, if the beam width and pad-to-pad distance are fixed (and the kink angle is adjusted by changing the length, as in figure 3), the maximum sensitivity is obtained for $\alpha \approx h/L$. This scenario (fixed h and L) is highly relevant, as h and L are often constrained by limits in lithography and release considerations.

It is worth noting that even asymptotically slender devices with large kink angles do not produce displacements that are comparable to buckle-type devices (unless one is interested in very small input strains).

3.4. Illustration: adsorption/temperature sensor design

The selective adsorption of molecules onto the surfaces of microfabricated devices is a well-established technique for biochemical sensing (e.g. see the reviews [8, 9]). The central concept is to translate surface stresses generated during adsorption into mechanical deformation; the modulus of the material factors heavily into this translation (see equation (2)). The prevalent approach is to use silicon cantilevers with $\sim$500 nm thickness, $\sim$500 μm lengths and $\sim$50 μm widths. For such devices, surface stresses in the range of 0.01–0.1 N m^{-1} yield displacements on the order of 10–100 nm.

In such applications, the kinked beam sensor has the notable advantage of not requiring one-sided adsorption (as

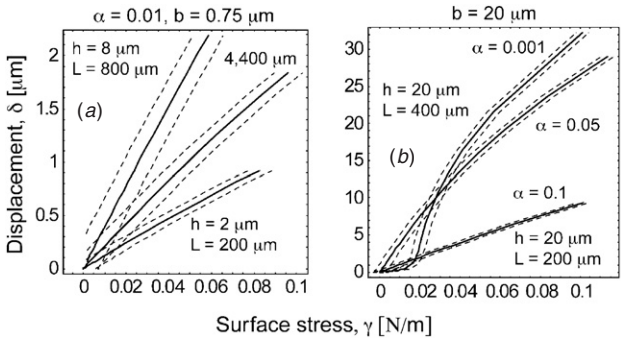

Figure 5. Theoretical displacements as a function of surface stress for two types of devices, with dashed lines to indicate the effects of temperature shifts: (*a*) PMMA with $E = 3$ GPa, CTE = 70 ppm $^{\circ}C^{-1}$, ± 0.1 $^{\circ}C$ temperature shifts, (*b*) PDMS with $E = 2$ MPa, CTE = 300 ppm $^{\circ}C^{-1}$, ± 1 $^{\circ}C$ temperature shifts.

required for cantilevers). Figures 5(*a*) and (*b*) illustrate theoretical displacements resulting from adsorption, for several devices made out of two different polymers commonly used in microfluidic devices. In figure 5(*a*) are the predictions for devices comprised of a glassy polymer, with properties typical of photoresist or poly(methylmethacrylate) (PMMA). The predictions in figure 5(*b*) are for devices comprised of a rubbery polymer, such as poly(dimethylsiloxane) (PDMS). The key distinction between these devices is their dramatically different elastic modulus, which implies that the input strain ε_o for a given surface stress γ will differ by orders of magnitude. The dimensions of the devices in these figures are consistent with the glassy polymer devices discussed elsewhere [3].

Figure 5(*a*) illustrates that glassy polymer[6] structures with dimensions typical of existing devices [3] will exhibit displacements that are an order of magnitude larger than silicon cantilevers of comparable dimensions. If existing polymeric kinked beam sensors are elongated—a highly feasible strategy considering the dry etching used to release such structures [3]—one can achieve displacements $>\sim 2$ μm. Of course, such sensors will be susceptible to temperature-induced deformation; the dashed lines in figure 5 represent the shifts that occur for a prescribed temperature shift. The glassy polymer is notably sensitive to temperature changes: 0.1 $^{\circ}C$ changes may lead to $\sim$250 nm of displacement. This implies that strict temperature control is required to eliminate the obfuscating effects of thermal expansion.

Conversely, the glassy polymer structure will be quite sensitive as a temperature sensor: temperature changes on the order of 1 $^{\circ}C$ translate into μm-scale displacements. One can reinterpret the abscissa as temperature by converting surface stress to equivalent temperature change using equation (2).

The right side of figure 5 illustrates that elastomers (such as poly(dimethylsiloxane)) create the opportunity to construct incredibly sensitive adsorption sensors. Here, the dramatic decrease in modulus results in displacements on the order of tens of microns—even for much wider, thicker and shorter devices. Moreover, the device with an extremely small kink angle holds the potential to distinguish between specific and non-specific adsorption. Non-specific adsorption (which usually involves physi-sorption as opposed to covalent bonding) leads to smaller surface stresses. With proper design, the buckle-type device can be constructed to exhibit very small displacements as a result of low surface stresses, yet large displacements for larger surface stresses generated by covalent bonding of specific species. Alternatively, if non-specific binding is not relevant, a small but finite kink angle results in a device that is highly sensitive to surface stress: such devices create the opportunity to measure surface stresses with unprecedented resolution.

Perhaps surprisingly, the PDMS device is less sensitive to temperature, despite its much larger CTE (300 ppm $^{\circ}C^{-1}$ as compared to 70 ppm $^{\circ}C^{-1}$ for the glassy polymer). The dashed lines represent 1 $^{\circ}C$ temperature shifts, which are an order of magnitude larger than those for the glassy polymer. The apparent temperature insensitivity of the PDMS device arises from the fact that the surface stress term in equation (2) dominates the thermal expansion term. Temperature-induced displacements are not small *per se* (indeed, they are on the order of microns), but rather are much smaller than those induced by adsorption.

It should be noted that very thin structures (whose planar thickness is much less than the beam width, h) will be prone to out-of-plane buckling, wherein the kinked beams deform out-of-plane. This will likely be the limiting factor in developing adsorption-based sensors. Neglecting the complicating factor of the kink in altering out-of-plane motion, the buckling threshold is defined by equation (19), with $\bar{b} \equiv b/L$ replacing $\bar{h}$. Finally, it should be noted that gravity may also promote out of plane motion which obfuscates output; however, the large surface-to-volume ratios of micro-devices typically implies that this deformation mode is negligible compared to the driving forces described above. Moreover, the use of fluidic environments further suppresses the effects of gravity, particularly for polymeric materials whose density is similar to that of common fluids.

4. Concluding remarks

The striking feature of the present analysis is that optimal sensor response is achieved by matching the kink angle with the aspect ratio of the kinked beam sensor arms. Strictly speaking, this rule only applies to sensors whose in-plane width and length are dictated *a priori*, such that the kink angle is the remaining design parameter. However, this is often indeed the case, as the beam width and length are typically governed by the microfabrication process; the minimum beam width is dictated by lithography limits, while the length is often constrained by release procedures and/or the desired size of the sensor. Sensors with this feature ($\alpha \approx h/L$) exhibit the greatest dynamic range, in the sense that high sensitivity is achieved for both small and large inputs. It is noteworthy that this extended dynamic range is a consequence of nonlinear behavior, even though the initial response for small input strains may be linear.

Alternatively, the kinked beam geometry presents the opportunity to construct buckling-type sensors that show little initial sensitivity, and then exhibit large deformations above a critical limit. This is particularly attractive for detection

[6] Examples include poly(methylmethacrylate) (PMMA) and many common photoresists [3].

scenarios wherein multiple physical inputs drive deformation, since it creates the opportunity to design sensors that are not prematurely 'triggered' by competing environmental factors. The nonlinear transition (from small to large deflections) can be modulated by adjusting the kink angle, provided that the precision of the microfabrication process is sufficient to produce very small kink angles reliably. In this context, non-zero kink angles can be more favorable than straight beams, because the asymmetry ensures directionality.

Acknowledgment

MRB gratefully acknowledges support from the National Science Foundation, via grant number CMS0529076.

References

[1] Gianchandani Y B and Najafi K 1996 Bent-beam strain sensors *IEEE J. Microelectromech. Syst.* **5** 52–8
[2] Que L, Gianchandani Y B and Cerrina F 1999 Mechanical characterization of electron-beam resist using micromachined structures *J. Vac. Sci. Technol.* **17** 2719–22
[3] Stanec J, Begley M R and Barker N S 2006 Mechanical properties of dehydrated photoresists for use in RF-MEMS applications *J. Micromech. Microeng.* **16** 2086–91
[4] Guo J, Suster M, Young D J and Ko W H 2005 High-gain mechanically amplified capacitive strain sensor *Sensors, 2005 IEEE Ann. Meeting* pp 464–7
[5] Stanec J, Smith C H, Chasiotis I and Barker N S 2007 Realization of low-stress Au cantilever beams *J. Micromech. Microeng.* **17** N7–10
[6] Begley M R 2005 The impact of material selection on the performance of microfabricated bilayer sensors and actuators *J. Micromech. Microeng.* **15** 2379–88
[7] Fang W and Wickert J A 1994 Post buckling of micromachined beams *J. Micromech. Microeng.* **4** 116–22
[8] Ettouhami A, Essaid A, Ouakrim N, Michel L and Limouri M 1996 Thermal buckling of silicon capacitive pressure sensors *Sensors Actuators* A **37** 167–71
[9] Suresh S and Freund B 2003 *Thin Film Materials* (Cambridge: Cambridge University Press)
[10] Carracosa L G, Morena M, Alvarez M and Lechuga L M 2006 Nanomechanical biosensors: a new sensing tool *Trends Anal. Chem.* **25** 196–206
[11] Raiteri R, Grattarola M, Butt H J and Skladal P 2001 Micromechanical cantilever-based biosensors *Sensors Actuators* B **79** 115–26